Acta Mech Sin (2007) 23:585–595
DOI 10.1007/s10409-007-0097-y

RESEARCH PAPER

J_2 invariant relative orbits via differential correction algorithm

Ming Xu · Shijie Xu

Received: 10 July 2006 / Revised: 26 March 2007 / Accepted: 2 April 2007 / Published online: 6 September 2007

Abstract This paper describes a practical method for finding the invariant orbits in J_2 relative dynamics. Working with the Hamiltonian model of the relative motion including the J_2 perturbation, the effective differential correction algorithm for finding periodic orbits in three-body problem is extended to formation flying of Earth's orbiters. Rather than using orbital elements, the analysis is done directly in physical space, which makes a direct connection with physical requirements. The asymptotic behavior of the invariant orbit is indicated by its stable and unstable manifolds. The period of the relative orbits is proved numerically to be slightly different from the ascending node period of the leader satellite, and a preliminary explanation for this phenomenon is presented. Then the compatibility between J_2 invariant orbit and desired relative geometry is considered, and the design procedure for the initial values of the compatible configuration is proposed. The influences of measure errors on the invariant orbit are also investigated by the Monte–Carlo simulation.

Keywords Formation flying · J_2 invariant orbit · Differential correction · Formation configuration

1 Introduction

Formation flying problem (FFP) of satellites has attracted much attention of researchers in recent years. Since the relative motion of satellite formations is very complicated, many works have been devoted to simplifying the relative dynamics to better understand the relative motion [1–6]. Most of them are based on the non-perturbed Keplerian orbits. In fact, the presence of the disturbances between satellites (e.g., J_2 term, relative drag) will lead to drift in a formation. And it is uneconomical to counteract the drift just by means of the active control. Therefore, the study about the relative dynamics associated with the perturbations has more extensive perspective [1].

The dominant J_2 oblateness effect in perturbations is considered as the main destroyer to the formation configuration [1–3]. And J_2 invariant orbit is firstly defined by Schaub and Alfriend [1] in mean orbital elements to minimize the amount of fuel to maintain. Then Li et al. [2,3] concluded, from the point of view of relative orbital elements, that the drifts of relative orbit result from the orbital inclination and right ascension of ascending node of the two satellites. Zhang and Dai [4] removed the drifts by adjusting the semi-axis of the follower satellite and obtained a similar conclusion. However, all the above works are based on the mean orbital elements instead of the Cartesian coordinates, which prevents the J_2 invariant orbit from being applied.

By means of Routh transformation and dynamical system theory, Koon and Marsden [5] developed a method to find the J_2 invariant orbit. Kasdin and Koleman [6] studied the Hamilton model of relative motion with leader satellite (Leader) orbit of zero inclination, and suggested to describe the periodic relative motion using canonical epicyclic orbital elements. Biggs et al. [7] proposed a method to determinate the J_2 invariant orbit with the leader's orbit of zero inclination based on the targeting method in chaos dynamics.

So far, FFP is considered only in the field of Restricted Two Body Problem (R2BP) or perturbed R2BP. Actually, the relative motion is a degeneration of Circular Restricted Three Body Problem (CR3BP) when the mass radio $\mu \to 0$ [8]. So some technologies developed for Halo orbits (a class

The project supported by the Innovation Foundation of Beihang University for Ph.D. Graduates, and the National Natural Science Foundation of China (60535010).

M. Xu (✉) · S. Xu
School of Astronautics, Beihang University, Beijing 100083, China
e-mail: xumingle@gmail.com

of periodic orbits in CR3BP) may be applied to FFP. For example, Richardson [9] attained the third order expansion for FFP, just as he did for Halo orbit in 1980.

Motivated by the idea above, the authors of this paper will extend the differential correction (DC) algorithm for finding Halo orbit [10,11] in CR3BP to FFP of Earth's orbiters for searching the J_2 invariant orbit. Rather than using orbital elements, the analysis is based on the Hamiltonian form in physical space, which makes a direct connection with physical requirements. The invariant manifolds (stable and unstable manifold) are used to indicate the asymptotic behavior of the invariant orbit. It is demonstrated that the period of the orbit is slightly different from the ascending node period of the leader satellite. Then the formation remain in the particular configuration is considered. The design procedure is proposed to create the initial values of the compatible configuration. The influence of measure errors upon DC is investigated by the Monte–Carlo simulation.

The DC algorithm developed in this paper can obtain the real-time velocity required by the J_2 invariant orbit from the measure information, so it can be used in the autonomous formation flying. Similarly, the long-term correction can be used to design the compatible formation configuration.

2 Hamiltonian model for relative motion dynamics

2.1 Coordinate definition

(a) Orbital reference frame for the leader satellite (SLO): the origin O is set at the leader; X_O axis is in the direction from the Earth's center to the leader; Z_O axis is in the direction of the orbital momentum moment of the leader; Y_O axis is determined by the right-hand rule.
(b) Inertial reference frame for the geocentric-equator (SEI): the origin O is set at the Earth's center; X_I axis points to the vernal equinox; Z_I is along the spin axis of the Earth; Y_O is determined by the right-hand rule. The sketch map of relative motion in SLO is shown in Fig. 1.

2.2 J_2 absolute dynamics

Denote that u is the argument of latitude; i is the orbital inclination; Ω is the right ascension of ascending node; L is the magnitude of the orbital momentum moment; p is the semi-latus rectum. The orbital elements in this paper are referred to the leader's without any exception.

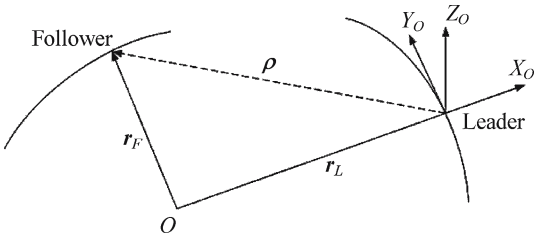

Fig. 1 Sketch map of relative motion in SLO

Under the effect of J_2 perturbation, $u, i, L, r_L, \boldsymbol{r}_L, \boldsymbol{v}_L$ of the leader can be obtained numerically. So $\dot{r}_L$, $\dot{\Omega}$, $\dot{i}$ are as following:

$$\dot{i} = \frac{r_L \cos u}{\sqrt{\mu p}} \cdot f_h, \tag{1}$$

$$\dot{\Omega} = \frac{r_L \sin u}{\sqrt{\mu p} \sin i} \cdot f_h, \tag{2}$$

$$\dot{u} = \frac{L}{r_L^2} - \dot{\Omega} \cos i, \tag{3}$$

$$\dot{r}_L = \frac{x_L}{r_L}\dot{x}_L + \frac{y_L}{r_L}\dot{y}_L + \frac{z_L}{r_L}\dot{z}_L = \frac{\boldsymbol{r}_L \cdot \boldsymbol{v}_L}{r_L}, \tag{4}$$

$$f_h = -\frac{3J_2 R_e^2 \mu}{2r_L^4} \cdot \sin 2i \sin u, \tag{5}$$

where $\boldsymbol{r}_L$ is the position vector of the leader; r_L is the magnitude of $\boldsymbol{r}_L$; $\boldsymbol{v}_L$ is the velocity vector of the leader in SEI; R_e is the Earth's radius; μ is the gravitational constant of the Earth; J_2 is the second order zonal coefficients of gravitational potential.

Integrating Eqs. (1)–(5) will achieve high precisions for the short-term calculation, but will accumulate the integral errors for the long-term calculation. So the analytic theory for orbital perturbation is available for the long-term integration with lower precision requirement.

2.3 J_2 relative dynamics

The kinematics of the follower relative to the leader is

$$\boldsymbol{r}_F = \boldsymbol{r}_L + \boldsymbol{\rho}, \tag{6}$$

$$\boldsymbol{v}_F = \boldsymbol{v}_L + \boldsymbol{\omega} \times (\boldsymbol{r}_L + \boldsymbol{\rho}) + \frac{\mathrm{d}^O}{\mathrm{d}t}\boldsymbol{\rho}, \tag{7}$$

where $\boldsymbol{r}_F$ is the position vector of the follower; $\boldsymbol{\rho}$ is the position vector of the follower relative to the leader with its components $[x\ y\ z]^{\mathrm{T}}$ in SLO; $\boldsymbol{v}_F$ is the inertial velocity of the follower; $\boldsymbol{\omega}$ is instantaneous angle velocity vector of the leader; $\frac{\mathrm{d}^O}{\mathrm{d}t}$ means differentiating with respect to the time in SLO. The instantaneous angle velocity $\boldsymbol{\omega}$ has the form in SLO as

$$(\boldsymbol{\omega})_O = \boldsymbol{R}_z(u)\boldsymbol{R}_x(i)\begin{bmatrix}0\\0\\\dot{\Omega}\end{bmatrix} + \boldsymbol{R}_z(u)\begin{bmatrix}\dot{i}\\0\\0\end{bmatrix} + \begin{bmatrix}0\\0\\\dot{u}\end{bmatrix}, \tag{8}$$

where $\boldsymbol{R}_z(\theta)$ and $\boldsymbol{R}_x(\theta)$ are the elementary transformation matrixes around Z and X axis, respectively. And $\boldsymbol{r}_F$ has the form in SEI as

$$(\boldsymbol{r}_F)_I = \boldsymbol{R}_z(-\Omega)\boldsymbol{R}_x(-i)\boldsymbol{R}_z(-u)\begin{bmatrix}r_L + x\\y\\z\end{bmatrix}, \tag{9}$$

where $r_F = \|\boldsymbol{r}_F\| = \sqrt{(r_L + x)^2 + y^2 + z^2}$.

Expanding the third component of Eq. (9) yields

$$(z_F)_I = (r_L + x)\sin u \sin i + y \cos u \sin i + z \cos i. \quad (10)$$

The follower's kinetic energy is

$$K = \frac{1}{2}(\boldsymbol{v}_F)^{\mathrm{T}}(\boldsymbol{v}_F) \quad (11)$$

and its potential energy is

$$U = -\frac{\mu}{r_L} + \frac{\mu J_2 R_e^2}{2r_F^3}\left[3\frac{(z_F)_I^2}{r_F^2} - 1\right], \quad (12)$$

then its Lagrange function is

$$L' = K - U. \quad (13)$$

The generalized momentum is defined as $p = \frac{\partial K}{\partial \dot{\rho}}$, namely

$$\begin{aligned} p_x &= \dot{x} + z(\cos u \sin i\dot{\Omega} - \sin u\dot{i}) \\ &\quad - y(\cos i\dot{\Omega} + \dot{u}) + \dot{r}_L, \\ p_y &= \dot{y} + (r_L + x)(\cos i\dot{\Omega} + \dot{u}) \\ &\quad - z(\sin u \sin i\dot{\Omega} + \cos u\dot{i}), \\ p_z &= \dot{z} + y(\sin u \sin i\dot{\Omega} + \cos u\dot{i}) \\ &\quad - (r_L + x)(\cos u + \sin i\dot{\Omega} - \sin u\dot{i}), \end{aligned} \quad (14)$$

then the Hamiltonian function is

$$\begin{aligned} H = \sum_{x,y,z} \rho_i p_i - L' &= -\frac{p_x^2}{2} - \frac{p_y^2}{2} - \frac{p_z^2}{2} \\ &+ p_x[p_x - z(\cos u \sin i\dot{\Omega} - \sin u\dot{i}) \\ &+ y(\cos i\dot{\Omega} + \dot{u}) - \dot{r}_L] \\ &+ p_y[p_y - (r_L + x)(\cos i\dot{\Omega} + \dot{u}) \\ &+ z(\sin u \sin i\dot{\Omega} + \cos u\dot{i})] \\ &+ p_z[p_z - y(\sin u \sin i\dot{\Omega} + \cos u\dot{i}) \\ &+ (r_L + x)(\cos u + \sin i\dot{\Omega} - \sin u\dot{i})] \\ &- \frac{\mu}{[(r_L + x)^2 + y^2 + z^2]^{1/2}} + \frac{J_2 R_e^2 \mu}{2} \\ &\cdot\{3[(r_L + x)\sin u \sin i + y \cos u \sin i + z \cos i]^2 \\ &- (r_L + x)^2 - y^2 - z^2\}\big/[(r_L + x)^2 + y^2 + z^2]^{5/2}, \end{aligned} \quad (15)$$

where $u, i, r_L, \dot{r}_L, \dot{\Omega}, \dot{i}$ are the time explicit functions determined by the J_2 absolute dynamics of the leader.

Choosing the state vector $\boldsymbol{X} = [x, y, z, p_x, p_y, p_z]^{\mathrm{T}}$, the J_2 relative dynamics has the brief form as

$$\dot{\boldsymbol{X}} = \mathrm{J}\nabla_X H, \quad (16)$$

where J is a symplectic operator, and $\nabla_X H$ is the gradient vector of H.

Hereto, the Hamiltonian model for J_2 relative dynamics has been constructed without any simplified assumptions, and the Lagrange or Newtonian model can be also constructed by the similar process. The model constructed here will have extraordinarily precision in stationkeeping control and state estimations.

It is the Hamiltonian model that has the advantage of requiring only one-order ordinary differential equations, while both the Lagrange and Newtonian models need second order differentials from the leader. Especially for the long-term design, the symplectic integrator just based on Hamiltonian system will retard the energy dissipation, which is another advantage of the Hamiltonian model.

2.4 Perturbed period

According to the J_2 absolute dynamics, the oscillating period of elements u, a, e, i is termed the ascending-node period $T_d = \int_0^{2\pi} \frac{\mathrm{d}t}{\mathrm{d}u}\mathrm{d}u$; the oscillating period of $r, \dot{r}$ is notated T_r; the mean orbital period is $\bar{T} = 2\pi\sqrt{\bar{a}^3/\mu}$, where $\bar{a} = \frac{1}{2\pi}\int_0^{2\pi} a(u)\mathrm{d}u$ is the mean semi-axis. Generally, T_d, T_r and $\bar{T}$ have little difference:

$$\begin{aligned} \Delta_1 &= \left|\frac{T_r - T_d}{T_d}\right| \sim O(10^{-4}), \\ \Delta_2 &= \left|\frac{\bar{T} - T_d}{T_d}\right| \sim O(10^{-4}). \end{aligned} \quad (17)$$

3 Existence and denseness of invariant orbit

3.1 Existence

According to [1] and [2], the existent condition for the J_2 invariant orbit is

$$\begin{aligned} &\delta T_d = 0, \\ &\delta[(\Delta\Omega)_{2\pi}] = 0, \end{aligned} \quad (18)$$

whose first-order expansion is

$$\begin{aligned} &f_i(\delta\bar{a}, \delta\bar{i}, \delta\bar{e}) = 0, \quad i = 1, 2, \\ &\delta\bar{\Omega}, \delta\bar{\omega}, \delta\bar{M} \text{ arbitrary}, \end{aligned} \quad (19)$$

where f_i are the linear combinations of $\delta\bar{a}, \delta\bar{i}, \delta\bar{e}$. The detailed expressions of f_i can be found in [1] and [2]. The little difference in geometry between the leader and the follower can be expressed as the variation on the leader's elements

and coordinates, namely

$$\delta\Delta = \Delta_{\text{follower}} - \Delta_{\text{leader}}, \quad \Delta = \bar{a}, \bar{i}, \bar{e}, \bar{\Omega}, \bar{\omega}, \bar{M}, x, y, z. \tag{20}$$

The more strict condition for the J_2 invariant orbit is that all the elements have the same excursing rate, namely,

$$\begin{aligned} &\delta\bar{a} = 0, \delta\bar{i} = 0, \delta\bar{e} = 0, \\ &\delta\bar{\Omega}, \delta\bar{\omega}, \delta\bar{M} \text{ arbitrary.} \end{aligned} \tag{21}$$

The relative position vector of the follower relative to the leader can be expressed as the variation of the leader's position vector. And the position vector of the leader has the form in SEI as

$$\begin{bmatrix} x_i \\ y_i \\ z_i \end{bmatrix} = \begin{bmatrix} \cos u \cos\Omega - \sin u \cos i \sin\Omega \\ \cos u \sin\Omega + \sin u \cos i \cos\Omega \\ \sin u \sin i \end{bmatrix} \cdot \frac{a(1-e^2)}{1 + e\cos\theta}, \tag{22}$$

where all the orbital elements are osculating elements.

Taking the variation for Eq. (22) yields

$$\begin{aligned} \delta \begin{bmatrix} x_i \\ y_i \\ z_i \end{bmatrix} = &\begin{bmatrix} -\sin u \cos\Omega\delta u - \cos u \sin\Omega\delta\Omega - \cos u \cos i \sin\Omega\delta u - \sin u \cos i \cos\Omega\delta\Omega \\ -\sin u \sin\Omega\delta u + \sin u \cos\Omega\delta\Omega + \cos u \cos i \cos\Omega\delta u - \sin u \cos i \sin\Omega\delta\Omega \\ \cos u \sin i\,\delta u \end{bmatrix} \\ &\cdot \frac{a(1-e^2)}{1 + e\cos\theta} + \begin{bmatrix} \cos u \cos\Omega - \sin u \cos i \sin\Omega \\ \cos u \sin\Omega + \sin u \cos i \cos\Omega \\ \sin u \sin i \end{bmatrix} \cdot \frac{a(1-e^2)}{(1 + e\cos\theta)^2} e \sin\theta\delta\theta + O(\delta a, \delta i, \delta e). \end{aligned} \tag{23}$$

It is obvious that both the relative orbits given in Eqs. (19) and (21) have the same period T_d. The Poincaré section (PS) of relative orbits deduced from Eq. (21) is shown in Fig. 2 (Poincaré Mapping will be defined in Sect. 4.1). The PS has no fix points or closed curves, so there is no rigorous periodic or quasi-periodic orbits in relative orbits, which is consistent to the conclusion of "the relative orbit is not periodic, but bounded for the short terms of a, e, i" given in [1] and [2].

3.2 Denseness

Theorem *The invariant orbit is dense in some domain; it means that any point in position space will stay on some invariant orbit.*

Proof We just need to prove that the relative position vector of invariant orbit can distribute arbitrarily in inertial reference frame.

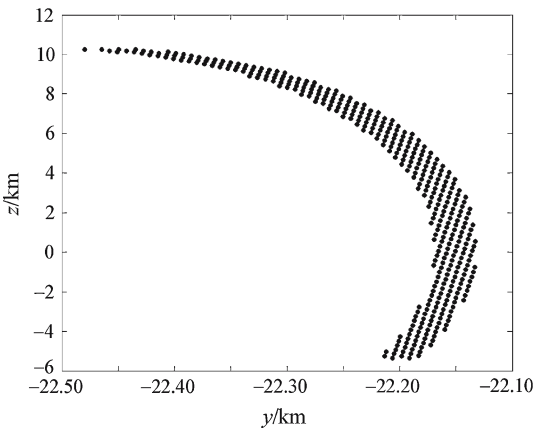

Fig. 2 Poincaré section

According to Eq. (19) or (21), $\delta\Omega, \delta\omega, \delta M$ for the invariant orbit are arbitrary, so $\delta[x_i \ y_i \ z_i]^{\mathrm{T}}$ has an arbitrary distribution in some domain. Therefore, the theorem proof is complete.

Remark 1 The denseness guarantees the existence of the J_2 invariant orbit on any point, but not the uniqueness.

4 Differential correction

The initialization procedure of FFP is as follows: the follower is long-rangely guided to the neighborhood of the leader, and then the velocity impulse (1st correction) required by the invariant orbit makes the follower fly in the desired formation. The autonomous strategy of stationkeeping for FFP is as following: the follower deviates from the invariant orbit after periods of time, and then the velocity impulse (2nd correction) derived from the real-time measure information makes the follower return formation fly again.

Due to the denseness of the invariant orbit, any position in physical space can be used for invariant formation. So the desired velocity in formation is just decided by the position. The following text will give a correction algorithm aiming at the velocity generation.

4.1 Correction algorithm

Definition of Poincaré Mapping (see Fig. 3) Poincaré section Σ is taken at $\boldsymbol{X} = [x_0\ 0\ 0\ 0\ 0\ 0]^{\mathrm{T}}$, and the mapping $\boldsymbol{P}$ is defined as

$$\forall \boldsymbol{X}_0 \in \Sigma, \quad \boldsymbol{X}_f = \boldsymbol{P}(\boldsymbol{X}_0) = \boldsymbol{\phi}_{T^*}(\boldsymbol{X}_0),$$

where $\boldsymbol{\phi}$ is the flow; T^*, the interval that the orbit intersects Σ twice, is termed Poincaré period in this paper.

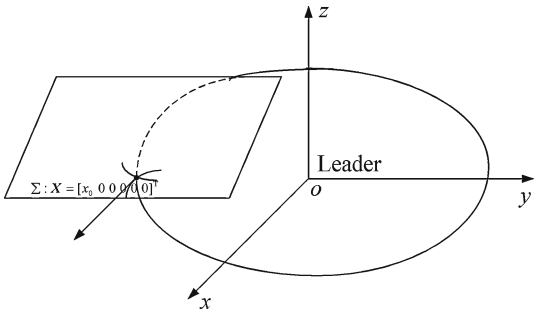

Fig. 3 Sketch of the Poincaré Mapping

Then the variation equation for the J_2 relative dynamics is as follows

$$\dot{\boldsymbol{\Phi}}(t) = J\frac{\partial^2 H}{\partial \boldsymbol{X}^2}\boldsymbol{\Phi}(t), \qquad \boldsymbol{\Phi}(0) = \boldsymbol{I}_{6\times 6}. \tag{24}$$

The monodromy matrix for the invariant orbit is defined as

$$\boldsymbol{\Phi}(T^*) := \boldsymbol{\Phi}(t)|_{t=T^*}$$

$\boldsymbol{\Phi}(T^*)$ has the equivalent definition as

$$\boldsymbol{\Phi}(T^*) := \frac{\partial \boldsymbol{\phi}_t(\boldsymbol{X}_0)}{\partial \boldsymbol{X}_0}\Big|_{t=T^*} = \frac{\partial \boldsymbol{X}(T^*)}{\partial \boldsymbol{X}(0)}. \tag{25}$$

Differentiating the Poincaré Mapping yields

$$\mathrm{d}\boldsymbol{X}_f = \boldsymbol{\phi}_{T^*+\mathrm{d}T}(\boldsymbol{X}_0 + \mathrm{d}\boldsymbol{X}_0) - \boldsymbol{\phi}_{T^*}(\boldsymbol{X}_0). \tag{26}$$

Ignoring the second orders and expanding this in Taylor series yield

$$\mathrm{d}\boldsymbol{X}_f = \boldsymbol{\Phi}(T^*)\mathrm{d}\boldsymbol{X}_0 + \frac{\partial \boldsymbol{X}}{\partial t}\Big|_{t=T}\mathrm{d}T, \tag{27}$$

i.e.,

$$\begin{aligned}&[0 \quad \mathrm{d}y_f \quad \mathrm{d}z_f \quad \mathrm{d}p_{xf} \quad \mathrm{d}p_{yf} \quad \mathrm{d}p_{zf}]^{\mathrm{T}}\\ &\quad = \boldsymbol{\Phi}(T)[0 \quad 0 \quad 0 \quad \mathrm{d}p_{x0} \quad \mathrm{d}p_{y0} \quad \mathrm{d}p_{z0}]^{\mathrm{T}}\\ &\qquad +[\dot{x}_f \quad \dot{y}_f \quad \dot{z}_f \quad \dot{p}_{xf} \quad \dot{p}_{yf} \quad \dot{p}_{zf}]^{\mathrm{T}} \cdot \mathrm{d}T,\end{aligned} \tag{28}$$

expanding the first element of Eq. (28) yields

$$\mathrm{d}x_f = \Phi_{14}\mathrm{d}\dot{x}_0 + \Phi_{15}\mathrm{d}\dot{y}_0 + \Phi_{16}\mathrm{d}\dot{z}_0 + \dot{x}_f\mathrm{d}T = 0. \tag{29}$$

Define

$$\boldsymbol{Z} := [\mathrm{d}y \quad \mathrm{d}z \quad \mathrm{d}p_x \quad \mathrm{d}p_y \quad \mathrm{d}p_z]^{\mathrm{T}}, \tag{30}$$

$$\boldsymbol{M} := \begin{bmatrix} \Phi_{24} & \Phi_{25} & \Phi_{26} \\ \vdots & \vdots & \vdots \\ \Phi_{64} & \Phi_{65} & \Phi_{66} \end{bmatrix}_{5\times 3}, \tag{31}$$

then the correction is

$$\mathrm{d}\tilde{\boldsymbol{V}}_0 = [\mathrm{d}p_{x0} \quad \mathrm{d}p_{y0} \quad \mathrm{d}p_{z0}]^{\mathrm{T}}. \tag{32}$$

It is seen from Eq. (14) that $\mathrm{d}\tilde{\boldsymbol{V}}_0$ is just the physical velocity correction $\mathrm{d}\boldsymbol{V}_0 = [\mathrm{d}\dot{x}_0\ \mathrm{d}\dot{y}_0\ \mathrm{d}\dot{z}_0]^{\mathrm{T}}$. Therefore, the velocity correction should satisfy the following condition

$$-\boldsymbol{Z}_f = \left\{\boldsymbol{M} + \frac{1}{\dot{x}_f}\frac{\partial \boldsymbol{Z}}{\partial t}\Big|_f [\Phi_{14} \quad \Phi_{15} \quad \Phi_{16}]\right\}\mathrm{d}\tilde{\boldsymbol{V}}_0. \tag{33}$$

Denote

$$\boldsymbol{D} := \boldsymbol{M} + \frac{1}{\dot{x}_f}\frac{\partial \boldsymbol{Z}}{\partial t}\Big|_f [\Phi_{14} \quad \Phi_{15} \quad \Phi_{16}] \tag{34}$$

from Eq. (33), one can get the pseudo inverse solution of Eq. (34)

$$\mathrm{d}\tilde{\boldsymbol{V}}_0 = -(\boldsymbol{D}^{\mathrm{T}}\boldsymbol{D})^{-1}\boldsymbol{D}^{\mathrm{T}}\boldsymbol{Z}_f \tag{35}$$

the correction for T^* is

$$\mathrm{d}T = -\frac{1}{\dot{x}_f}[\Phi_{14} \quad \Phi_{15} \quad \Phi_{16}]\mathrm{d}\boldsymbol{V}_0. \tag{36}$$

4.2 Convergency

DC algorithm is essentially a modification of Newton iteration algorithm to solve the non-linear equation

$$\boldsymbol{F}_{5\times 1}(\boldsymbol{V}_0) = 0. \tag{37}$$

The convergent condition for the correction algorithm given in Sect. 4.1 is the existence and denseness for the J_2 invariant orbit. The initial value for iterations should be near the true value. Then executing 2–4 iterations will give the required corrections. The existence conditions for unperturbed periodic orbit can be used as the initial guess for the 1st correction, and the result of 1st correction can be used as the initial guess for the 2nd correction.

For the formation with large eccentricity, the initial guess can be found via the Lawden equations; for the formation with small eccentricity, the existence conditions for the periodic orbit in C-W equations can be used as the initial guess

$$\begin{aligned}&\dot{y}_0 = -2\omega x_0,\\ &\dot{x}_0 = \frac{1}{2}\omega y_0,\\ &\dot{z}_0 \text{ arbitrary},\end{aligned} \tag{38}$$

where ω is the angle velocity of the leader.

Associating with the existence and denseness for the J_2 invariant orbit, $x_0y_0z_0$ and $\dot{z}_0$(to be corrected) will give the uniqueness of the J_2 invariant orbit. So the J_2 invariant orbit has four-degree of freedom (DOF, namely, $x_0y_0z_0$ and $\dot{z}_0$), which matches Eq. (19) (the DOF are $\delta\bar{\Omega}$, $\delta\bar{\omega}$, $\delta\bar{M}$ and one of $\delta\bar{a}$, $\delta\bar{e}$, $\delta\bar{i}$).

In order to make the invariant orbit drift more slowly, we can improve the correction algorithm: the **Poincaré Mapping** is redefined as

$$\forall \boldsymbol{X}_0 \in \Sigma, \quad \boldsymbol{X}_f = \boldsymbol{P}(\boldsymbol{X}_0) = \boldsymbol{\phi}_{N\cdot T^*}(\boldsymbol{X}_0),$$

Table 1 Instantaneous orbital elements of the lead satellite

a m	e	i (°)	Ω (°)	ω (°)	θ (°)
6,971,004	0.005	97.73	10	30	95

where $N \cdot T^*$ is the interval when the orbit intersects the Poincaré section Σ after N times.

The correction algorithm can be termed N-Periodic Correction (N-DC), and its initial guess can be the result of 1-DC ($N = 1$).

4.3 Numerical simulation

The instantaneous orbital elements of the leader are listed in Table 1, the relative initial values of the follower is listed in Table 2 where the excursions before and after corrections are also listed.

The results in Table 2 can be recapitulated as follows:

(1) The excursion in along-track velocity is restrained for the correction. The more iteration times the correction has, the fewer excursions the along-track velocity has.
(2) The Poincaré section Σ chosen at the Plane $\boldsymbol{X} = [x_0\ 0\ 0\ 0\ 0\ 0]^{\mathrm{T}}$ means that the quadrature is terminated at no excursion in the radial direction, and the correction will weaken the excursion in the along-track and out-of-plane directions. Thus the excursion in the radial direction results just from the numerical errors, which can be weakened by the smaller step size in the quadrature.
(3) The trajectories evolving during 20 Poincaré periods are showed in Fig. 4 (the dashed line represents the trajectories without correction, the real line represents the trajectories with correction, and the asterisk represents the initial position). The trajectories have only the excursion of 42.6 m during 20 Poincaré periods (14 km for the case without correction).
(4) The excursion during 400 Poincaré periods after 1-DC is 2.1075 km (266.17 km for the case without correction).
(5) In the case of long-term DC, the large N will make the Matrix M in Eq. (31) so large that it may lead the correction algorithm to diverge. So its initial guess in this case will have more rigorous restriction, and step-by-step correction is an effective method. It means that one can start from short-term DC, and use the result from short-term DC as the initial guess of long-term DC. The correction for $N = 400$ in this paper follows the process

$$\text{C-W} \rightarrow 25\,\text{DC} \rightarrow 50\,\text{DC} \rightarrow \cdots \rightarrow 375\,\text{DC} \rightarrow 400\,\text{DC}.$$

The final excursion for this process is 222.2964 m.
(6) Just from the algorithm's point of view, the correction sequence may extend to the larger N. However, from the physical point of view, other ignored perturbations, such as J_3 and J_4 terms, atmospheric drag, Sun and Moon perturbing acceleration, may accumulate together, which will make the correction invalid.

5 Period and stability of invariant orbit

5.1 Period of invariant orbit

According to the theory of spectrum analysis, the Hamiltonian function can be expanded as follows

$$H = H_0 + \varepsilon_1 H_1 + \varepsilon_2 H_2 + \cdots, \tag{39}$$

where H_0 is just the Kepler motion (with period $\bar{T}$); H_1 is the periodic oscillations in u, a, e, i caused by J_2 (with period T_d); and H_2 is the periodic oscillations in $r, \dot{r}$ (with period T_r). Obviously, $\varepsilon_1 = O(J_2)$, and $\varepsilon_2 = O(J_2) \cdot O(\dot{\omega}) = O(J_2^2)$.

Table 2 Initial relative condition and DC of the follow satellite

Case	x_0 (m)	y_0 (m)	z_0 (m)	$\dot{z}_0$ (m s^{-1})	Poincaré period T (s)	Excursions before and after correction ($\Delta_{\mathrm{CW}}/\Delta_{\mathrm{Correction}}$)			Correction ΔV (m s^{-1})		
						Δx (m)	Δy (m)	Δz (m)	X	Y	Z
1	1,000	−15,000	−1,500	−0.05	5,800.125	−0.53/ − 0.71	−734.40/ − 0.0064	−5.61/ − 0.011	0.026	−0.042	−0.919
2	15,000	1,000	1,500	0.1	5,800.125	0.025/0.04	710.31/0.10	5.38/ − 0.004	0.021	0.041	0.869
3	−1,500	−1,000	15,000	−0.1	5,800.125	−0.013/ − 0.01	−140.00/ − 0.24	59.15/0.57	0.237	−0.016	0.981
4	1,000	−15,000	−1,500	−0.05	5,800.125 × 20	−4.48/ − 4.14	-1.4×10^4/40.45	−93.35/12.75	0.026	−0.042	−0.919
5	1,000	−15,000	−1,500	−0.05	5,800.125 × 400	-1.4×10^4/ − 5.86	-2.66×10^5/2,084	−1, 518.2/ − 317.4	0.026	−0.042	−0.919
6	1,000	−15,000	−1,500	−0.05	5,800.125 × 400	-1.4×10^4/ − 0.38	-2.66×10^5/ − 222.3	−1, 518.2/ − 0.32	6.876	−0.053	−0.206

The excursions in Cases 1–3 are the ones during 1 Poincaré period after 1-DC, the excursion in Case 4 is the one during 20 Poincaré periods after 1-DC, the excursion in Case 5 is the one during 400 Poincaré periods after 1-DC, and the excursion in Case 6 is the one during 400 Poincaré periods after 400-DC

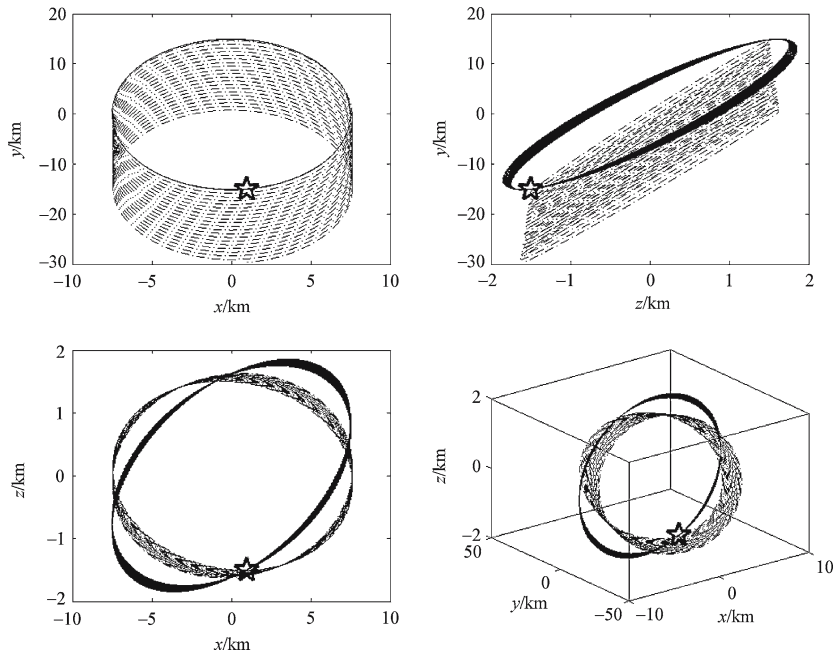

Fig. 4 Evolvement of the J_2 invariant orbit

According to the definition of Poincaré Mapping, the period for the relative orbit is the Poincaré period $T^* = 5{,}800.125$ s; the mean orbital period for the leader can be attained via its mean orbital elements, $\bar{T} = 5{,}796.3$ s; numerically integrating the J_2 relative dynamics in 50 mean periods, one obtains $T_d = 5{,}803.5$ s, $T_r = 5{,}800.0$ s. It is obvious that T^* is more close to T_r than T_d, and here we will give the elementary explain for the phenomenon in the follows [12]:

Without the consideration of J_2 perturbation, the system H_0 will have the periodic solutions whose period is $\bar{T}$ (whether the different ellipse orbits have the periodic relative motions just depends on if they have the same semi-axis). There are still the periodic solutions for the system H_0 associating with the periodic disturbance $\varepsilon_1 H_1$. However, the solution's period becomes the period T_d due to the disturbance. In the similar manner, the system $H_0 + \varepsilon_1 H_1$ will associate with the periodic disturbance $\varepsilon_2 H_2$, so the period of the remaining periodic solutions becomes T_r.

All the process is similar to the forced vibrations of a mechanical spring, but the rigorous proof needs more advanced mathematical theories, which will be introduced in our another paper.

5.2 Stable and unstable manifolds

Hamiltonian theory indicates that $\boldsymbol{\Phi} = \mathrm{D}_z \boldsymbol{P}(z)$, the differential of $\boldsymbol{P}(z)$, is the symplectic matrix. By means of the numerical technique, one can abtain the eigenvalues of $\boldsymbol{\Phi}$: $|\lambda|_i = 1, i = 1, 2, 3, 4, \lambda_5 = \lambda_6^{-1} > 1$. So the invariant orbit abtained by DC has the 4D center manifolds (with the eigenvalues $\lambda_i, i = 1, 2, 3, 4$), 1D stable manifolds (with the eigenvalues λ_6), and 1D unstable manifolds (with the eigenvalues λ_5). One branch of stable and unstable manifolds of the periodic orbit is shown in Fig. 5 (light-colored surface represents the stable manifolds, and deep colored surface represents the unstable manifolds).

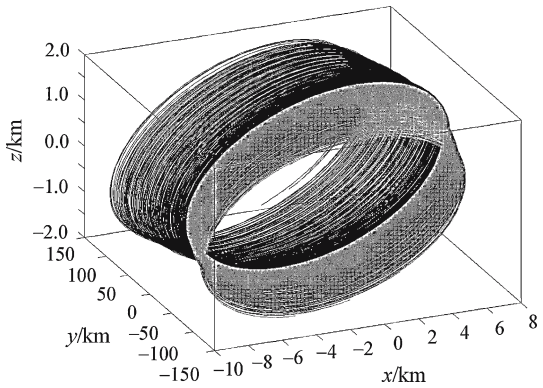

Fig. 5 A branch of stable and unstable manifolds of relative periodic orbit

Similar to the asymptotic behavior of Halo orbit, the stable and unstable manifolds have significant applications in formation initialization, reconfiguration and deconstruction: the follower can tend to the invariant orbit along the stable manifolds with few fuel consumptions, and can also depart from the invariant orbit along the unstable manifolds at the end of formation mission.

6 Compatibility between J_2 invariant orbit and formation configuration

6.1 Formation configuration

The leader and the follower should fly in some configuration to fulfil a prescript mission. The usual configurations are spatial circularity, subpoint circularity, coplanar ellipse, and so on [13].

According to the C-W equations, the solution to the relative motion in spatial circularity ($x^2 + y^2 + z^2 = R^2$) is as follows

$$\begin{aligned} x &= \frac{R}{2}\cos(\omega t + \alpha), \\ y &= -R\sin(\omega t + \alpha), \\ z &= \pm\sqrt{3}x, \end{aligned} \tag{40}$$

where R is the radius of the spatial circularity, and α is the initial phase angle at the time $t = 0$.

Notate $\theta = \omega t + \alpha$. Then only one DOF ($\theta$) is necessary to determine the relative motion (with R known). Here only the J_2 invariant orbit in spatial circularity configuration is investigated, and the cases for subpoint circularity and coplanar ellipse can be achieved similarly.

6.2 Compatibility definition

The J_2 invariant orbit abtained via DC at any point P on the configuration may be quite different from the desired orbit (as the worst case, the two orbits may be nearly vertical with each other). Meng [13] illustrated the difficulty of maintaining the formation configuration and the J_2 invariant orbit at the same time. Meng [14] considered that the destruction of the J_2 perturbation to formation configuration can be rejected for some given inclinations of the leader.

The compatibility between the J_2 invariant orbit and the formation configuration at point P is defined as the similarity of them. So the more similar they are, the better compatibility they have, and vice versa.

Define the compatibility parameter of point P as $C(P)$, i.e.,

$$C(P) := \frac{\sqrt{\left(\max\limits_{(x,y,z)\in J_2\text{I.O.}(N)} \sqrt{x^2+y^2+z^2} - R\right)^2 + \left(\min\limits_{(x,y,z)\in J_2\text{I.O.}(N)} \sqrt{x^2+y^2+z^2} - R\right)^2}}{R},$$

where J_2 I.O.(N) represents the J_2 invariant orbit obtained via the N-DC. The smaller $C(P)$ is, the better compatibility they have, and vice versa.

The procedure to obtain the distribution of C-P and the compatible configuration is shown as follows:

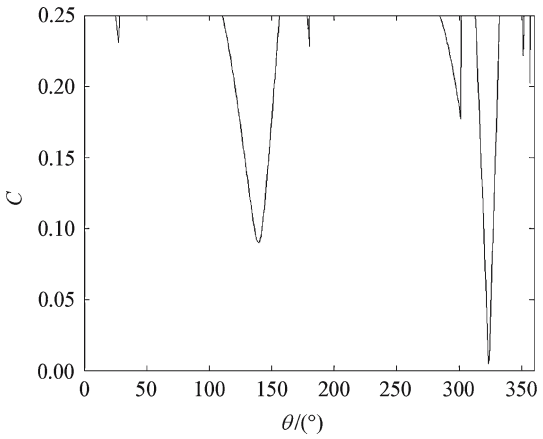

Fig. 6 Distribution of C-P

for $\theta = 0$–$360°$

Step 1: transform θ into $(x, y, z, \dot{x}, \dot{y}, \dot{z})$ on the basis of Eq. (39), namely $\theta \to (x, y, z, \dot{x}, \dot{y}, \dot{z})$;
Step 2: use N-DC on the point to give the velocity correction ΔV and its J_2 invariant orbit;
Step 3: calculate the compatibility parameter $C(P)$;

end
plot the distribution of C-P;
the points satisfying the given compatibility (or the extremum of $C(P)$) and their J_2 invariant orbits are the expected ones.

Figure 6 shows the distribution of compatibility parameter C vs. P (with correction period $N = 1$, the orbital elements for the leader is chosen as same as in Sect. 4.3, and the radius of the spatial circularity R is 20 km). It is seen that the distribution of C-P has the characters of uncontinuity, of no analytic expression, and of multiple humps.

Plotting the distribution of C-P will cost lots of calculations. Furthermore, in most of cases, one needs to get the minimum of C-P only, not the total distribution. So the random search method, for example, Genetic Algorithm (GA), is suitable to solve the extremum problem like the distribution of C-P. The cost function for the problem is just $C(P)$, and the parameter to be optimized is θ. The mature GA Toolbox in MATLAB7.0 can deal with this work, so the details are neglected here.

6.3 Numerical simulation

The instantaneous orbital elements of the leader are as same as in Table 1; the initial conditions are determined by Eq. (40)

Table 3 Relative initial condition and DC of the follower

Case	Poincaré period	Excursions before and after correction ($\Delta_{CW}/\Delta_{Correction}$)			Correction ΔV ($m\,s^{-1}$)			Consistency parameter
	T (s)	Δx (m)	Δy (m)	Δz (m)	X	Y	Z	C
7	5,800.125	3.14/0.47	$760/-2.9\times10^{-4}$	$4.67/1.18\times10^{-2}$	0.0199	0.00988	−0.0812	0.0034
8	$5{,}800.125\times50$	756/0.84	$8.57\times10^{4}/195.36$	$-160.70/-34.66$	0.722	−0.0456	−0.621	0.0470

The excursion in Case 7 is the one during 1 Poincaré period after 1-DC, and the excursion in Case 8 is the one during 50 Poincaré periods after 50-DC

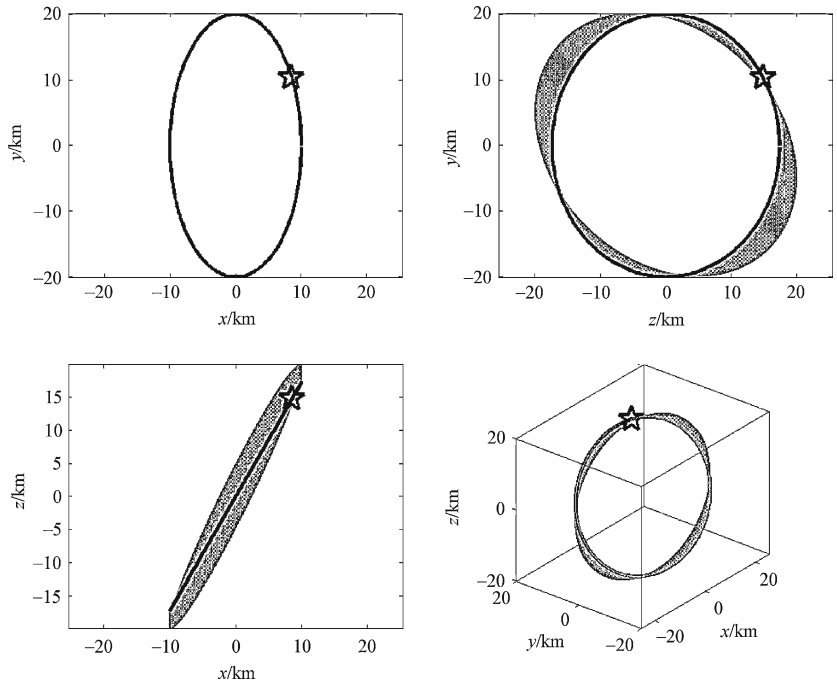

Fig. 7 Evolvement of compatible spatial-circular configuration

with $\theta = 323.1°$; the radius of the spatial circularity R is 20 km. The excursions and corrections ΔV's after 1-DC or 50-DC are shown in Table 3.

The results in Table 3 can be recapitulated as follows:

(1) The excursion is just 0.4757 m during 1 Poincaré period after 1-DC (Case 7), and 198.4101 m during 50 Poincaré periods after 50-DC (Case 8).
(2) Trajectories evolving during 50 Poincaré periods are showed in Fig. 7 (the light-colored line represents the J_2 invariant orbit, the deep colored line represents the ideal configuration, and asterisk marks the initial position). The trajectories are slightly distorted under the J_2 perturbation.
(3) The distance between the leader and the follower during 50 Poincaré periods is shown in Fig. 8. The formation configuration is destroyed gradually, but the destruction in 50 Poincaré periods is so tiny that the compatibility parameter C only increases from 0.0034 to 0.047.

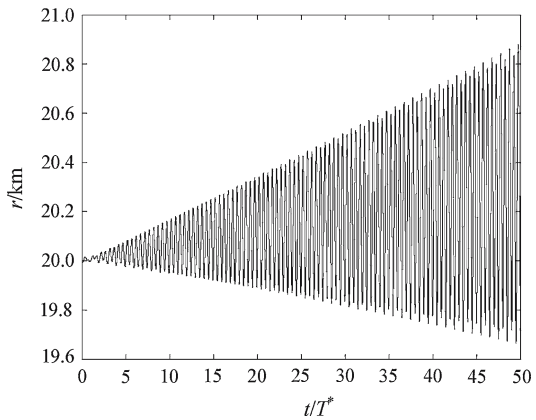

Fig. 8 Distance r between the leader and the follower

7 Influences of measure errors on correction

7.1 Dispersion error analysis

In engineering practice, the orbit determination error E_1 of the leader and the relative navigation error E_2 will have an

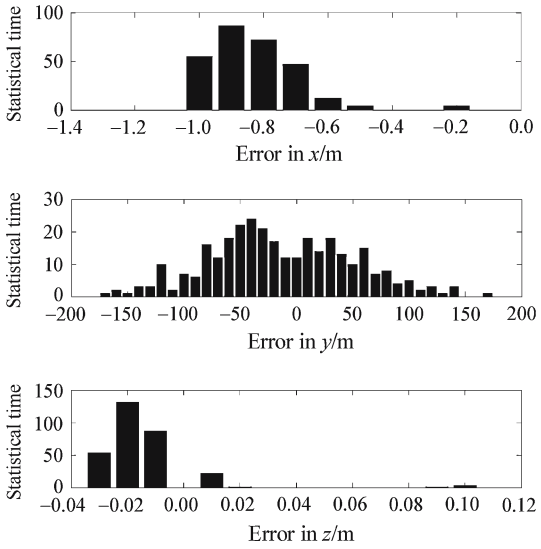

Fig. 9 Error distributions in position

Table 4 Confidence level

Confidence (%)	Error distribution (m)		
	X	*Y*	*Z*
90	0.8747	104.76	0.0150
95	0.9217	123.72	0.0176
99	0.9695	148.23	0.0974

adverse influence on the correction results. In this paper, E_1 and E_2 are supposed to obey the Gauss distributions. Their means are all zeros. The variances (1σ) are 50 m in position and 0.01 m/s in velocity for E_1, and 0.1 m in position and 0.005 m/s in velocity for E_2. The measure precisions of the leader's orbit determination and relative navigation can be achieved by GPS and space-borne radars or other devices [15].

7.2 Monte–Carlo simulation

E_1 and E_2 will make the correction results random. Therefore, the Monte–Carlo simulation involving 250 iterations is used to investigate the statistical error dispersions of correction results. Error distributions in position are shown in Fig. 9 (errors in magnitude and direction), and confidence levels are shown in Table 4 (errors just in magnitude).

From the simulation, we find that the measure errors have the main influence on the Y axis, secondary on X and Z axis. So the stationkeeping for the invariant orbit is necessary.

8 Conclusions

This paper dealt with the J_2 invariant orbits for formation flying. The Hamiltonian model for relative motion including the J_2 perturbation was constructed without any simplified assumption. The DC method developed for finding periodic orbits (Halo orbits) in CR3BP was extended to the formation flying. Thereby, a new method of searching the J_2 invariant orbits was obtained. The method is suitable for the measure and control operation in a formation flying mission since the Cartesian coordinates are adopted. The stable and unstable manifolds were calculated to indicate the asymptotic behavior of the relative periodic orbits, which can be used to initialize, reconfigure or deconstruct the formation. A preliminarily theoretical analysis was given to explain why the period of the relative orbits via DC is different from the ascending node period of the leader. Then the compatibility between the J_2 invariant orbit and the formation configuration was proposed, accompanied with the design procedure for the initial guess of the compatible configuration. The statistical dispersion analysis was performed by the Monte–Carlo simulation.

The research shows that the J_2 relative dynamics and DC may give the required velocity on-line for the invariant orbit according to the real-time measure. So the research results can be used to autonomous formation flying. Moreover, the long-term correction can be used to design the compatible formation configuration. However, orbit determination and relative navigation errors will destroy the correction results, which will increase the fuel consumption for maintaining formation. The measure errors are still the barrier for the engineering practice in formation flying.

References

1. Schaub, H., Alfriend, K.: J_2 invariant relative orbits for spacecraft formations. Celestial Mech. Dyn. Astron. **79**, 77–95 (2001)
2. Meng, X., Li, J., Gao, Y.: J_2 perturbation analysis of relative orbits in satellite formation flying. Acta Mech. Sin. **38**(1), 89–96 (2006, in Chinese)
3. Li, X., Li, J.: Study on relative orbital configuration in satellite formation flying. Acta Mech. Sin. **21**(1), 87–94 (2005)
4. Zhang, Y., Dai, J.: Satellite formation flying with J_2 perturbation. J. Nat. Univ. Defense Technol. **24**(2), 6–10 (2002, in Chinese)
5. Koon, W.S., Marsden, J.E.: J_2 dynamics and formation flight. In: AIAA Guidance, Navigation, and Control Conference and Exhibit, Montreal, Canada, AIAA 2001–4090 (2001)
6. Kasdin, N.J., Koleman, E.: Bounded, periodic relative motion using canonical epicyclic orbital elements. In: Proceedings of AAS/AIAA Space Flight Mechanics Meeting, Copper Mountain, Colorado, AAS 05–186 (2005)
7. Biggs, J.D., Becerra, V.M.: A search for invariant relative satellite motion. In: 4th Workshop on Satellite Constellations and Formation Flying, Sao Jose dos Campos, Brazil, pp. 203–213 (2005)
8. Liu, L., Wang, H.: Problem about the formation flying of the constellation's small satellites. Acta Astron. Sin. **45**(1), 57–67 (2004, in Chinese)
9. Richardson, D.L., Mitchell, W.: A third-order analytical solution for relative motion with a circular reference orbit. In: AAS/AIAA Space Flight Mechanics Meeting, San Antonio, Spain, AAS02-147 (2002)

10. Popescu, M., Cardos, V.: The domain of initial conditions for the class of three-dimensional halo periodical orbits. Acta Astron. **36**, 193–196 (1995)
11. Xu, M., Xu, S.: The application of libration points and halo orbits in the earth–moon system to space mission design. Chin. J. Astron. **27**(4), 695–699 (2006, in Chinese)
12. Sansone, G., Conti, R.: Nonlinear Differential Equations. Pergamon Press, Oxford (1964)
13. Meng, X.: Formation design and perturbations of satellite formation flying based on relative orbital elements. Doctor Dissertation, Tsinghua University, Beijing (2005)
14. Meng, Y., Dai, J.: Analysis of stability, simulation and configuration design for satellite formation under the influence of the J_2 perturbation. J. Syst. Simul. **17**(2), 483–487 (2005)
15. Wei, C., Zhang, H.: Autonomous determination of relative orbit for formation flying satellites. Aerospace Control **3**, 41–47 (2003, in Chinese)